Nuclear Materials and Energy 23 (2020) 100745

Contents lists available at ScienceDirect

Nuclear Materials and Energy

journal homepage: www.elsevier.com/locate/nme

Nuclear loads and nuclear shielding performance of EU DEMO divertor: A comparative neutronics evaluation of two interim design options

J.H. You[a,*], R. Villari[b], D. Flammini[b], D. Marzullo[c], G. Mazzone[b]

[a] Max Planck Institute for Plasma Physics, Boltzmannstr. 2, 85748 Garching, Germany
[b] ENEA Frascati, Department of Fusion and Technology for Nuclear Safety, via E. Fermi 45, 00044 Frascati, Italy
[c] CREATE/University of Naples, Department of Industrial Engineering, Piazzale Tecchio 80, 80125 Napoli, Italy

ARTICLE INFO

Keywords:
DEMO
Divertor
Vacuum vessel
Neutronics
Shielding
Nuclear loads
Neutron damage

ABSTRACT

In a demonstrational fusion power plant (DEMO), divertor is supposed to protect vacuum vessel and superconducting magnets against neutron flux in the bottom region of the vessel. The vessel is subject to a strict design limit in irradiation damage dose and the magnets in nuclear heating power, respectively. Thus, the DEMO divertor must have the capability to protect sufficiently the vessel and the magnets against neutron flux being substantially stronger than in ITER.

In this paper, a first systematic neutronics study for the European DEMO divertor is reported. Results of the extensive assessment of key nuclear loading features (nuclear heating, irradiation damage & helium production) are presented for two optional concepts, namely, dome and shielding liner including minor geometrical variants. The shielding performance of the two competing design options is discussed together with the case of a bare cassette (no shielding), particularly in terms of damage dose compared with the design limits specified for the European DEMO.

It was found that both the dome and shielding liner were able to significantly reduce the nuclear loads in the cassette body and the vessel. The maximum damage dose at the end of the lifetime remained subcritical for the cassette body for both cases whereas it exceeded the limit for the vessel under the dome, but only locally on the surface underneath the pumping duct. But, the damage could be reduced below the limit for the vessel by increasing the size of the dome or by deploying the shielding liner. The most critical feature was the excessive damage occurring in the own body of the shielding components where the maximum damage dose in the steel heat sink of the dome and the shielding liner far exceeded the design limit at the end of the lifetime.

1. Introduction

Being in charge of critical operational functions such as removal of ash and impurity particles and (partial) exhaust of thermal power from plasma, the divertor is one of the most important in-vessel components in a fusion reactor [1,2]. Being located at the bottom region of a tokamak-type reactor, the divertor acts as a physical as well as functional interface between plasma edge and surrounding vacuum vessel (VV) near the lower port [3,4].

In a fusion power plant, such as demonstrational fusion reactor (DEMO), a divertor system will be subjected to extremely harsh loading environment characterized by high heat fluxes, particle bombardment, electromagnetic forces and neutron fluxes [5–7]. Particularly, neutron irradiation poses critical issues as it causes embrittlement of materials by lattice damage and transmutation (e.g. helium) [8–10]. Loss of toughness (or strength) leads to higher risk of uncontrolled brittle failure of a component impairing the structural integrity [11–13]. Further detrimental effects are thermal softening and thermal stresses of structural materials due to volumetric nuclear heating by gamma ray production [14,15]. In such a circumstance, powerful active cooling is needed at the cost of design complication [16,17].

Moreover, the divertor is supposed to protect the VV and magnets from neutron flux. For the VV of the European DEMO, SS316LN type steel (e.g. X2CrNiMo17-12-2) is considered as material [3]. The VV is subject to a specified design limit with regard to damage dose which is set as 2.75 dpa for the envisaged design life of 6 fpy (full power year) [3,4]. This limit dose is deemed feasible as recommended in the RCC-MRx AFCEN code (reduction in ductility: $<30\%$, fracture energy: >350 kJ/m^2) [18,19]. The magnets are very vulnerable to nuclear heating since only a slight increase of temperature (even a few degrees)

* Corresponding author.
E-mail address: you@ipp.mpg.de (J.H. You).

https://doi.org/10.1016/j.nme.2020.100745
Received 10 October 2019; Received in revised form 3 April 2020; Accepted 7 April 2020
Available online 20 April 2020

can destroy the superconducting state. Thus, divertor must have a capability to provide sufficient shielding to both the VV and magnets against neutron flux.

The huge fusion power (2 GW) of a DEMO power plant implies considerable nuclear loads in the in-vessel components [20]. Furthermore, the presence of a pumping duct in each cassette body and the large opening of the lower ports of the VV makes the effective shielding for the VV and magnets difficult. For assuring shielding, a proper shielding concept needs to be devised and verified.

In this paper, a first systematic neutronics study for the European DEMO divertor is reported focusing on shielding performance. Extensive nuclear loading features (nuclear heating, material damage and helium production) were investigated for two competing shielding concepts (dome vs. shielding liner). Results of the comparative assessments are presented. Note that the current study is based on the interim version of the European DEMO divertor CAD model created in 2016 in the framework of the EUROfusion Consortium (obsolete at present) [21]. Revision of the CAD model is currently ongoing [22], but the essential features of nuclear loading presented in this paper should be still indicative.

2. Shielding concepts and design models

Fig. 1 shows a CAD model illustrating (a) the outer form of a divertor cassette of the EU DEMO based on the DEMO plant CAD model released in 2016 and (b) a technical drawing. A detailed description of the cassette geometry is found elsewhere [7,21]. A duct opening is located in the middle part of the cassette body through which the fuel-ash mixture is pumped out by an adjacent vacuum pump. The presence of the pumping duct necessitates shielding against neutron to protect the underlying vacuum vessel. To this end, an umbrella-type component can be deployed to cover the duct. The shielding component should not hinder the gas flow through the duct to avoid reduced pumping efficiency. In the following, two options of shielding concept considered in the EUROfusion divertor project are briefly described.

2.1. Dome

The first shielding option is a water-cooled dome placed towards the X-point as illustrated in Fig. 2. The dome provides shadowing for the underlying pumping duct. Such a dome-type shielding component has already been employed for the ITER divertor where the main function of the dome umbrella is actually to increase the pressure of neutral gas [23].

The upper skin of the dome consists of plasma-facing components (PFCs) which have the form of a typical tungsten monoblock joined to a cooling pipe of CuCrZr alloy at the middle. The cross section geometry with dimensions is shown in Fig. 3. Assuming peak heat flux up to 5MW/m^2 during stationary operations, highly conductive copper alloy was applied for the heat sink. The surface side is armoured with 5mm thick tungsten. This kind of PFC concept has been qualified for high-heat-flux applications at least up to 20MW/m^2 [24]. The PFC protects the underlying supporting structure made of reduced activation steel (Eurofer) from heat fluxes. The cooling circuits of the dome (PFCs and steel body) are connected to those of the cassette body via pipes.

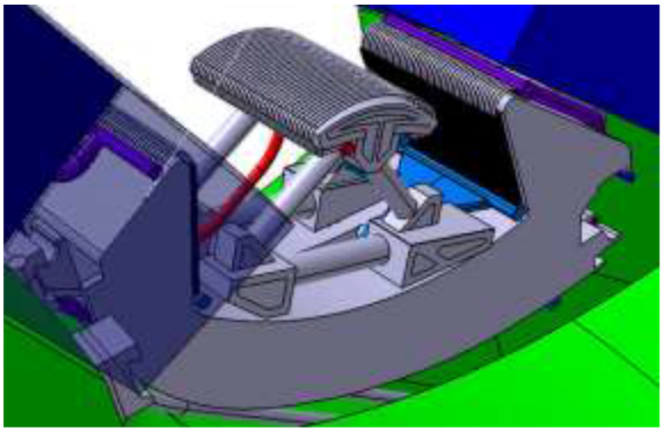

Fig. 2. 3D CAD model illustrating the geometry of the dome component installed at a divertor cassette.

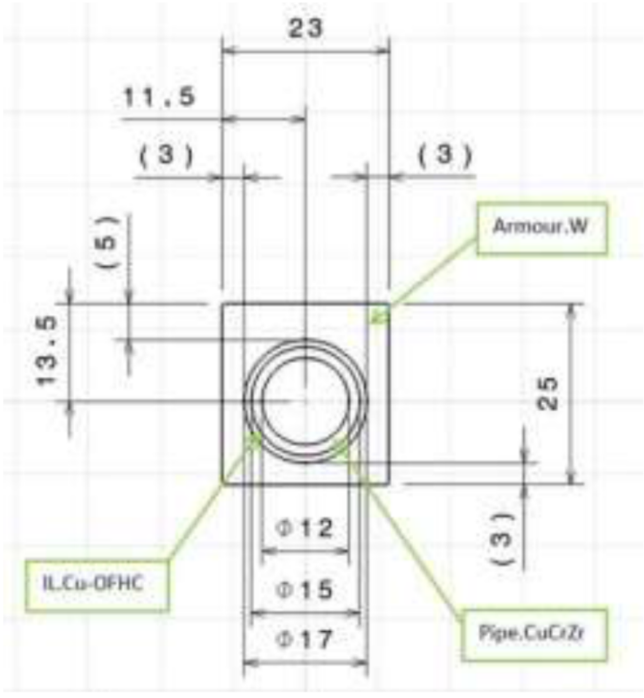

Fig. 3. Cross section geometry and dimensions of the dome PFCs.

For comparative assessments, three different variants of dome design were considered where two of them were equipped with extended wings (20cm and 40cm, respectively) attached to the cap while the other one without wing as illustrated in Fig. 4.

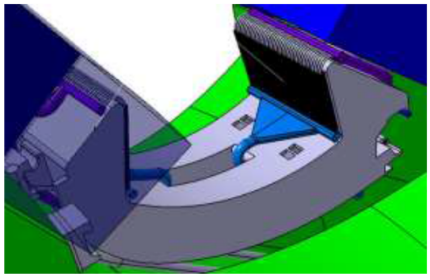

(a)

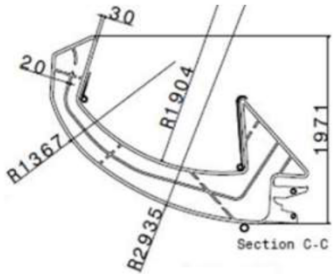

(b)

Fig. 1. (a) CAD model and (b) technical drawing illustrating the outer geometry of a divertor cassette designed for the EU DEMO plant model of the year 2016 [7,21].

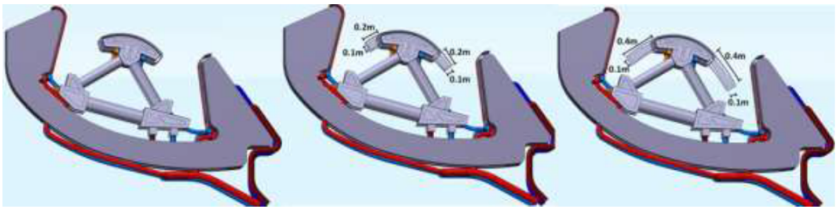

Fig. 4. Three different variants of divertor dome design: cap only (left), with a small (middle) and large wing extension (right), respectively.

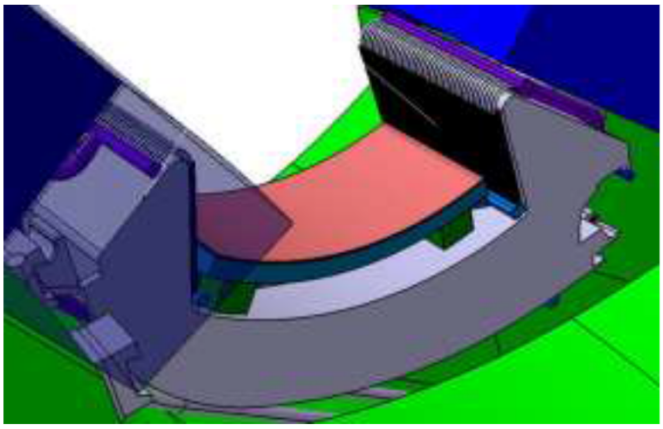

Fig. 5. 3D CAD model illustrating the geometry of the shielding liner component installed onto a divertor cassette.

2.2. Shielding liner

The second option is a shielding liner (SL) as illustrated in Fig. 5. The SL has a plate shape (either curved or flat) located directly above the cassette body. The height of the radial gap is defined by the compromise between two conflicting requirements: 1) allow sufficient toroidal gas flow for pumping and 2) reduce temperature increase due to nuclear heating in the supporting legs.

Fig. 6 shows the CAD models of the SL illustrating the poloidal (a) and toroidal (b) cross section. The dimensions are given in (c). The SL is designed as a water-cooled double deck heat sink structure made of Eurofer steel. The plasma-facing side is protected by 2mm thick tungsten armour. The upper cooling deck consists of a 10mm-thick steel plate containing a parallel array of small cooling tubes (diameter: initially 6mm, currently 8mm). The lower cooling deck has a thicker (50mm or 90mm) steel body featured by a parallel array of larger semicircle cooling channels (diameter: 80mm). The cooling circuit of the SL is connected to the cassette body via legs. This interim CAD model is subject to further optimization with regard to shielding and thermohydraulic performance.

2.3. Pumping duct size

One of the major factors affecting shielding performance is the size of duct opening. For a comparative assessment, three different duct opening sizes were considered as illustrated in Fig. 7. Note that the positions of the duct in Fig. 7 are slightly different to that of Fig. 1.

3. Neutronics models

3.1. Dome

The original CAD model of the divertor cassette system was post-processed using the CAD software SpaceClaim [25] to optimize void generation. Subsequently, the revised CAD model was converted to a geometry model for a Monte-Carlo N-Particle Transport (MCNP) code using the software MCAM [26]. Non-analytical surfaces were removed, complex bodies were segmented and the void space around the model was defined. The MCNP model consisted of 463 cells and 945 surfaces including voids. The developed MCNP model is shown in Fig. 8 (a-c). The MCNP model was validated with void runs to check for lost particles, where no lost particles were found in a test run with 1×10^8 particles. The materials assigned to the individual parts are defined in Table 1. For the sake of simplicity in computational modelling, the middle layer (indicated as light green layer in Fig. 8 c) of the PFCs of the dome and vertical targets was homogenized in terms of constituent materials (see Table 1).

3.2. Shielding liner

The procedure to create the MCNP model of the shielding liner was the same as described above. The MCNP model of the main cassette body was almost identical to that of Fig. 8 as well. The edge part of the MCNP model of the SL is shown in Fig. 9. The constitution of materials is defined in Table 2. The chemical composition of Eurofer97 is given in

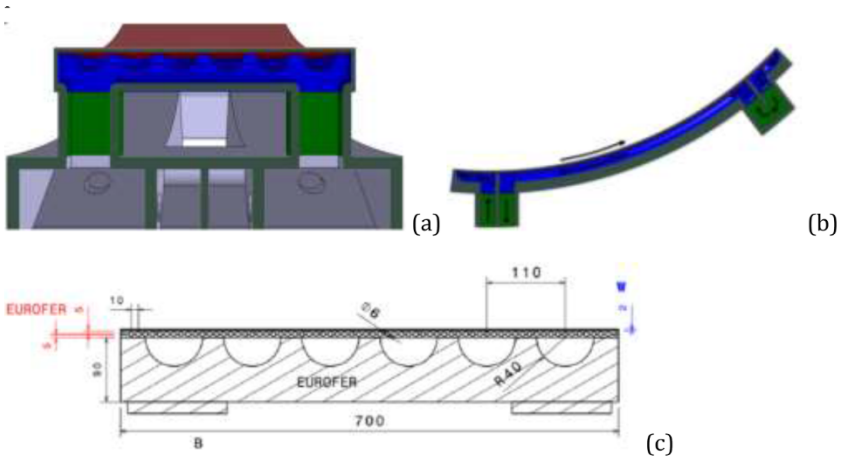

Fig. 6. CAD model images of the SLC illustrating the poloidal (a) and toroidal (b) cross sections and schematic drawing of the poloidal section showing the dimensions (c).

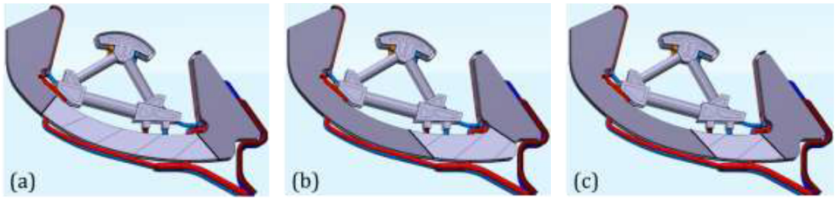

Fig. 7. Illustration of three different pumping duct configurations each with a different opening size, respectively. (a: large duct, b: medium size duct, c: small duct).

Table 3. Note that the maximum dose limit currently specified for Eurofer97 is 6 dpa at the inlet coolant temperature of 180°C. This limit was determined considering the FTTT (Fracture Toughness Transition Temperature) data measured for irradiated Eurofer steel tested at different doses and temperatures [8,27].

3.3. Vacuum vessel

The material of the VV is 316LN type stainless steel X2CrNiMo17-12-2 with controlled nitrogen (Cr: 17.5%, Ni: 12.5%, Mo: 2.5%, Mn: 2.0%, Si: 1.0%, C: 0.03) [8]. In the neutronics model, the solid shells of the VV are fully 316LN steel. The space between the shells is assumed to be a mixture of the steel (60 vol. %) and coolant (40 vol. %). The nuclear data are found in [28].

The lifetime of the VV was set at 6 fpy (with damage dose of 2.75 dpa) which was synchronized with that of the breeding blanket (Eurofer steel) where the maximum accumulated damage dose is expected to reach 70 dpa in the outboard equatorial region of the blanket [3,4].

3.4. Integration into a DEMO plant model (HCPB)

For a global 3D neutronics analysis on the plant scale, the MCNP model of the divertor cassettes were integrated into the 3D MCNP model of the HCPB (helium-Cooled Pebble Bed) DEMO plant model using the FILL card of MCNP. Fig. 10 shows the divertor region of the global MCNP model of the HCPB DEMO plant at two different toroidal angular positions respectively (a: with dome, b: bare cassette).

3.5. Neutronics analysis

3D neutronics calculations were carried out using MCNP5 and the JEFF 3.2 nuclear data [29,30]. The results were normalized to the assumed fusion power of 2037MW which corresponds to the neutron production rate of 7.2×10^{20} n/s. Mesh tallies (FMESH tally, voxel size: $5 \times 5 \times 5$ cm^3) with proper multipliers and standard cell-based energy deposition tallies (F6) were used [31].

4. Results and discussion

In this chapter, the results of neutronic analyses are presented in view of the radiation loads and shielding performance of the three considered design options (dome, 90mm SL, 50mm SL) in comparison with the case of no shielding (bare cassette). The radiation loading features were examined in terms of three major indicators, namely, nuclear heating, material damage and helium gas production by transmutation.

Table 1
Materials assigned to the MCNP model (in volume %).

	Color code	Constituent material(s)
Cassette body	light blue	Eurofer97
Dome body	light blue	Eurofer97
Coolant	dark blue	H_2O
Variable domains (dome wings, pumping duct)	orange	void or Eurofer(50%)/H_2O(50%)
PFC outer layers	Green	W
PFC middle layer	light green	W(34%), H_2O(33%), Cu(15%), CuCrZr(18%)

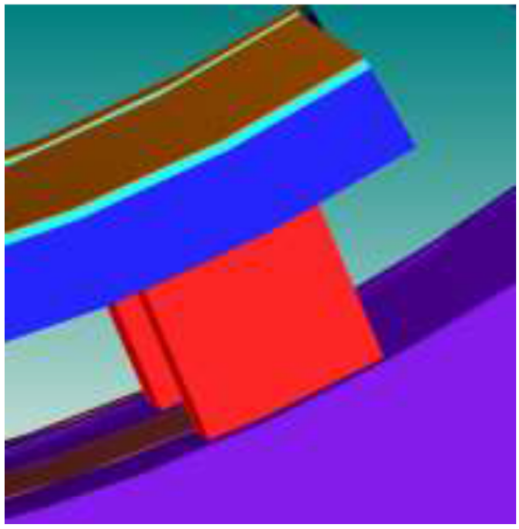

Fig. 9. The edge part of the MCNP model of the shielding liner.

Table 2
Materials constitution of the shielding liner component (in volume %).

	Color code	Constituent materials
Surface armor layer	Brown	W
Cooling substrate	Cyan	Eurofer(72%), H_2O(28%)
Main shield block	Blue	Eurofer(67%), H_2O(33%)
Supports	Red	Eurofer(60%), H_2O(40%)

4.1. Nuclear loading in the cassette body

4.1.1. Neutron flux

Fig. 11 shows the spatial distribution of neutron flux density emanating from the burning plasma into the divertor cassette. The front

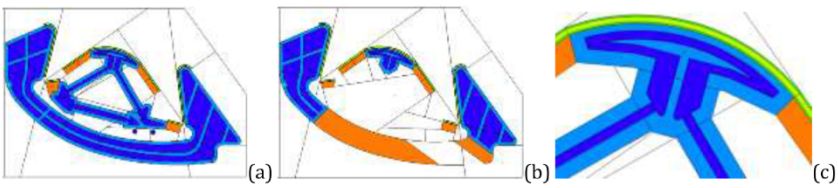

Fig. 8. MCNP model of the divertor cassette showing the poloidal cut section at 2° (a) and 6° (b), and close-up view of the dome (c). The colour code indicates different materials or material mixtures (navy blue: water, sky blue: steel, green: tungsten, light green: tungsten, copper and water, orange: either steel and water or empty).

Table 3
Chemical composition of Eurofer97 steel (wt.%) [8].

Fe	Cr	W	Mn	V	Ta	C	Ni	Mo	Ti	Nb	Al	B	Co
base	9	1.1	0.4	0.2	0.12	0.11	0.01	0.005	0.02	0.005	0.01	0.002	0.01

positions of the corresponding contour lines (plotted for 10^{13}, 10^{14} and $2{\cdot}10^{14}$ n/cm^{2}s, respectively) indicate the penetration density of neutron. The plots show that the contour lines are displaced towards the X-point in the presence of shielding components. For example, the contour lines of $2{\cdot}10^{14}$ n/cm^{2}s are running along the upper profile of the dome and the SL while the contour line reaches the surface of the bare cassette. This obviously reveals the shielding effect by the dome and the SL.

In Table 4, the maximum neutron flux density values in the cassette body (Eurofer steel) are given for six selected locations as indicated in Fig. 12. The result shows that the dome reduces the neutron flux down to below 40% in the central region while the SL down to 50-70% in the same region compared to the unprotected case.

4.1.2. Nuclear heating

In Fig. 13 the spatial distributions of volumetric thermal power density produced by nuclear heating are plotted in a logarithmic colour code scale. The figures clearly exhibit that the dome offers the most effective shielding for the cassette body whereas the dome itself experiences severe heating. The SL provides relatively modest shielding compared to the dome where the thickness of the steel block plays a minor role.

In Table 5, the maximum values of nuclear heating power density in the cassette body are given at the same six locations as in Fig. 12. As seen in Fig. 13, the maximum heating power occurs in the upper surface layer of the cassette body. For a quick comparison, the ratio to the corresponding values of the bare cassette is given in the parentheses. As revealed in Fig. 13, the dome offers the most effective shielding by up to a factor of three. The SL reduces the heating power down to 63%. On the inboard side, the edge region is hardly shielded under the SL and only moderately protected under the dome with a reduction of 17%. On the contrary, the outboard side is better protected. Near the outboard edge the heating power is reduced by 26-28% under the dome and the SL as well. The most significant shielding is reached in the middle part as expected. In this region, the heating power is reduced by 67% by the dome and 33% by the SLC. The two thicknesses of the steel block (90mm/50mm) makes a difference of up to 20% in heating power. It is recalled that it is the middle region of the cassette where the effectiveness of shielding is of critical concern because the pumping duct is located exactly there.

4.1.3. Material damage

Fig. 14 shows the spatial distributions of lattice damage generated by neutron irradiation in unit of dpa (displacement per atom) per one fpy in a logarithmic colour code. Note that the red colour filling the empty space is merely a numerical artefact. Similarly to the nuclear heating case shown in Fig. 13, the most effective protection is provided by the dome whereas the SL offers moderate shielding. The damage dose rapidly decays from the upper surface through the outward radial thickness.

In Table 6, the maximum damage dose in the cassette body is given at the same locations as in Fig. 12. It is seen that the inboard edge region tends to experience higher dpa damage than the outboard region. The middle part is effectively protected by the dome as well as the SL. It is recalled that the limit dose specified for the Eurofer steel is 6 dpa at the service temperature of 180°C (inlet coolant temperature for the cassette body). This means that cassette body requires shielding by either dome or SL in case a lifetime of longer than 2 fpy is pursued.

4.1.4. Helium production

Fig. 15 shows the spatial distributions of helium production rate by transmutation in unit of appm (atomic parts per million) per fpy together with contour lines of selected concentrations. As expected, the results exhibit the same qualitative trend as that of nuclear heating and dpa damage confirming significant shielding capability of the dome and SL.

Table 7 gives the maximum production rate of helium in the cassette body at the same locations as in Fig. 12. In the central region, the dome reduces the helium production down to 26-28% compared to the bare cassette and SL down to 48-69%. In the edge regions, particularly on the inboard side, the shielding effect is only marginal (even negative for SL).

It is remarkable that the amount of helium concentration to be produced in each fpy is generally quite large for all four cases. This might be a concern with regard to embrittlement of structural material (affecting the DBTT-behaviour of the ferritic-martensitic steel) and therefore structural analysis needs special care requiring a rigorous fracture mechanics treatment.

4.2. Nuclear loading in the vacuum vessel

An important measure of divertor shielding performance is the nuclear loads in the vacuum vessel. The estimated nuclear loads in the vessel are summarized in Table 8, 9 and 10, where nuclear heating power, damage dose and helium production at four selected positions (see Fig. 15) are given, respectively. The four positions selected here represent the regions of maximum nuclear loading. The data of interest are the values at 6 fpy (envisaged lifetime of the VV) given in parenthesis.

The damage dose values in Table 9 show that although notable

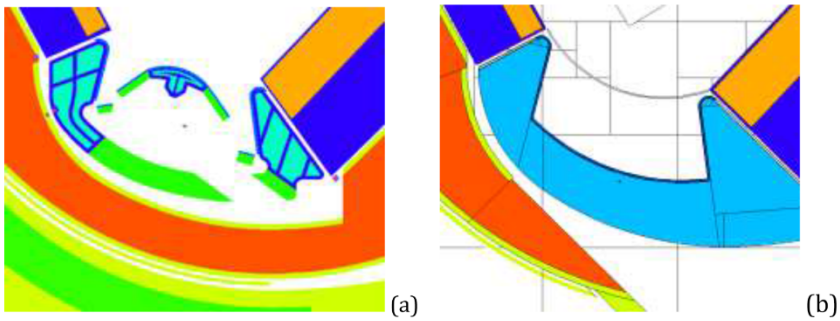

Fig. 10. Divertor region of the global MCNP model of the HCPB DEMO plant

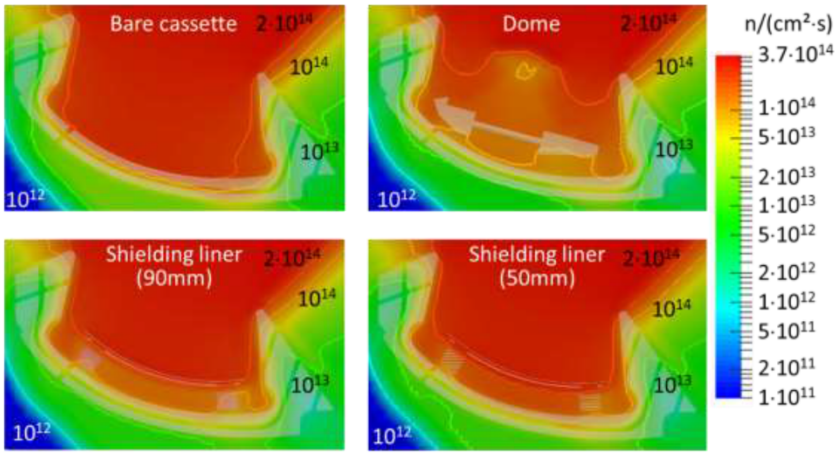

Fig. 11. Spatial distributions of neutron flux density radiating from the burning plasma into the DEMO divertor cassette. Results are presented for different cases of shielding design options.

Table 4
Maximum neutron flux density in the cassette body (Eurofer steel) at six selected locations as indicated in Fig. 12. The numbers in parenthesis indicate the ratios to the case of bare cassette.

(10^{14}·n/cm²·s)	Bare cassette	Dome	SLC (90mm)	SLC (50mm)
Inboard/shadow	1.9	1.5 (0.79)	1.6 (0.84)	1.7 (0.89)
Inboard/edge	2.2	1.7 (0.89)	1.5 (0.79)	1.7 (0.89)
Middle/shadow	2.3	0.9 (0.39)	1.2 (0.52)	1.5 (0.65)
Middle/edge	2.3	0.9 (0.38)	1.4 (0.58)	1.7 (0.71)
Outboard/shadow	1.5	1.0 (0.67)	1.0 (0.67)	1.1 (0.73)
Outboard/edge	1.5	1.0 (0.67)	1.0 (0.67)	1.1 (0.73)

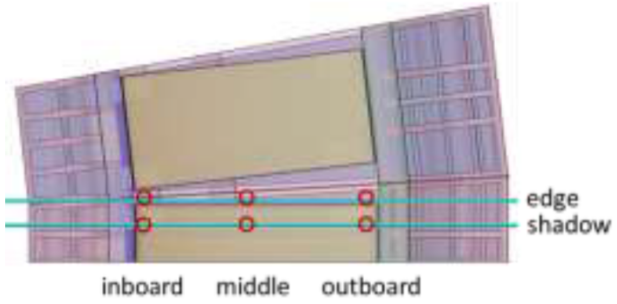

Fig. 12. Positions of the data selection for Table 4.

shielding effect can be achieved by both the dome and the SL at all locations, only the SL (with a thick or thin shield block) is able to provide sufficient protection for the vessel keeping the maximum damage below the required design criterion (2.75 dpa at 6 fpy). The damage in the region below the pumping duct (position 4) well exceeds the critical value even under the dome. For all cases, the maximum damage dose appears beneath the pumping duct, which is obviously due to the duct opening.

It is noted that the effectiveness of shielding depends on the coverage of the dome or the SL above the pumping duct. Thus, the results in Table 9 should be seen as an example from a first study made for the given geometric configuration and the shielding performance is to be further improved by optimizing the relative position and dimension of the pumping duct and shielding component. Generally, the SL offers better shielding compared to the dome. The vacuum vessel parts located directly beneath the cassette body are sufficiently protected even in the absence of any shielding component.

Another critical point is the considerable amount of helium produced by transmutation. As the recommended reweldability limit of helium concentration for a thick irradiated austenitic steel plate is <1 at.% [32], cutting and rewelding of the VV for refurbishment will not be possible.

4.3. Nuclear loading in the shielding components

Being the first firewall against neutron streaming, the shielding components (dome and SL) are likely to experience the harshest nuclear loads among the cassette system. Reliable shielding performance is assured only when the shielding components are operated within the allowable limit of nuclear loads.

In Table 11-13, the nuclear loads are summarized for the dome and the SL (with the 90mm and 50mm shield block), respectively. The positions where the results were estimated are indicated in Fig. 16.

Table 11 shows that the damage dose in the uppermost steel cap (position 1 and 2) of the dome well exceeds the design limit (6 dpa after 2 fpy) specified for Eurofer steel at the cassette cooling condition. On the contrary, the subjacent part of the dome below the cap (e.g. position 3 and 4) experiences much lower damage at uncritical levels. Significant amount of helium production is expected in the whole dome body, which may have impact on material toughness. Furthermore, the nuclear heating power in the steel cap is quite strong requiring effective cooling.

Table 12 and 13 show that the damage at the end of lifetime (2 fpy) in the steel substrate of the SL well exceeds the specified design limit (6 dpa). The damage in the shield block nearly reaches the critical value after 2 fpy. Such high dpa dose in the steel structure of the SL manifests that the thickness of the tungsten armour on the SL surface needs to be increased to reduce the neutron flux into the steel structure. As in the dome, a considerable amount of helium is produced in the steel body. The considerable amount of nuclear heating power in the SL implies that an effective cooling via dedicated cooling channels with a sufficiently large hydraulic diameter is required. First computational fluid dynamics simulation showed that the diameter of circular channels in the steel substrate should be at least 8mm or larger for achieving effective heat removal.

Comparison of the nuclear loads between Table 11 and Table 12-13 indicates that the SL is less loaded compared to the dome.

4.4. Impact of dome extension and pumping duct size on vessel damage

To assess the impact of component geometry on shielding effect, eight selected combinations of dome wing extension and duct opening sizes were investigated. For protecting the connectors of target pipework exposed at the lower edge areas of the targets, two baffle plates were optionally introduced as illustrated in Fig. 17. The design variants considered are as follows:

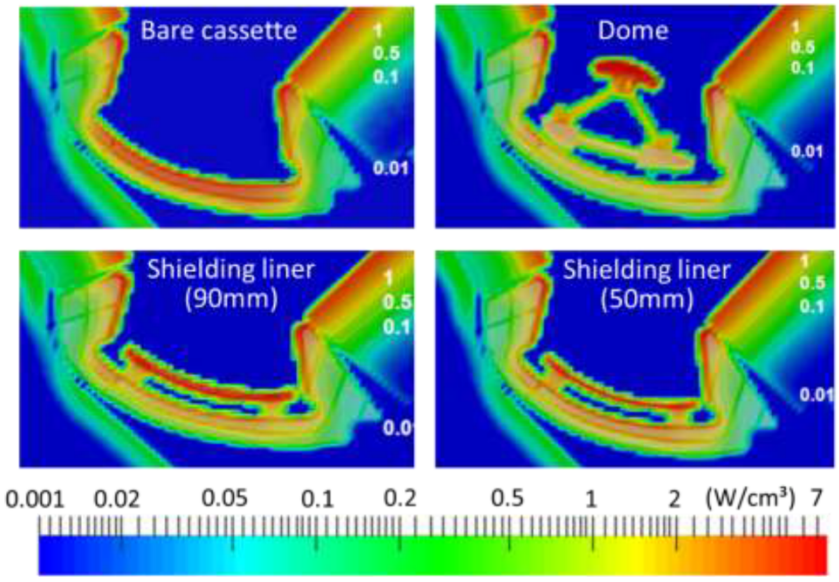

Fig. 13. Spatial distributions of volumetric thermal power produced by nuclear heating in the DEMO divertor cassette predicted for four different cases of design options.

Table 5
Maximum values of nuclear heating power density in the Eurofer steel cassette body at six selected locations indicated in Fig. 12. The numbers in parenthesis indicate the ratios to the bare cassette case.

(W/cm³)	Bare cassette	Dome	SLC (90mm)	SLC (50mm)
Inboard/shadow	4.6	3.8 (0.83)	4.4 (0.96)	4.6 (1.0)
Inboard/edge	4.1	3.4 (0.83)	4.0 (0.98)	4.2 (1.02)
Middle/shadow	7.0	2.5 (0.36)	4.4 (0.63)	5.4 (0.77)
Middle/edge	6.9	2.3 (0.33)	4.6 (0.67)	5.4 (0.78)
Outboard/shadow	4.3	3.1 (0.72)	3.2 (0.74)	3.6 (0.84)
Outboard/edge	4.4	3.2 (0.73)	3.2 (0.73)	3.6 (0.82)

Table 6
Irradiation damage dose in the cassette body at six selected locations indicated in Fig. 12. The numbers in parenthesis indicate the ratios to the bare cassette case.

(dpa/fpy)	Bare cassette	Dome	SLC (90mm)	SLC (50mm)
Inboard/shadow	2.3	2.0 (0.87)	2.1 (0.89)	2.2 (0.93)
Inboard/edge	2.5	2.1 (0.84)	2.3 (0.90)	2.3 (0.92)
Middle/shadow	3.3	0.8 (0.23)	1.5 (0.44)	2.0 (0.59)
Middle/edge	3.4	0.8 (0.22)	1.8 (0.52)	2.2 (0.66)
Outboard/shadow	1.8	1.3 (0.71)	1.3 (0.74)	1.5 (0.83)
Outboard/edge	1.7	1.3 (0.74)	1.2 (0.71)	1.4 (0.79)

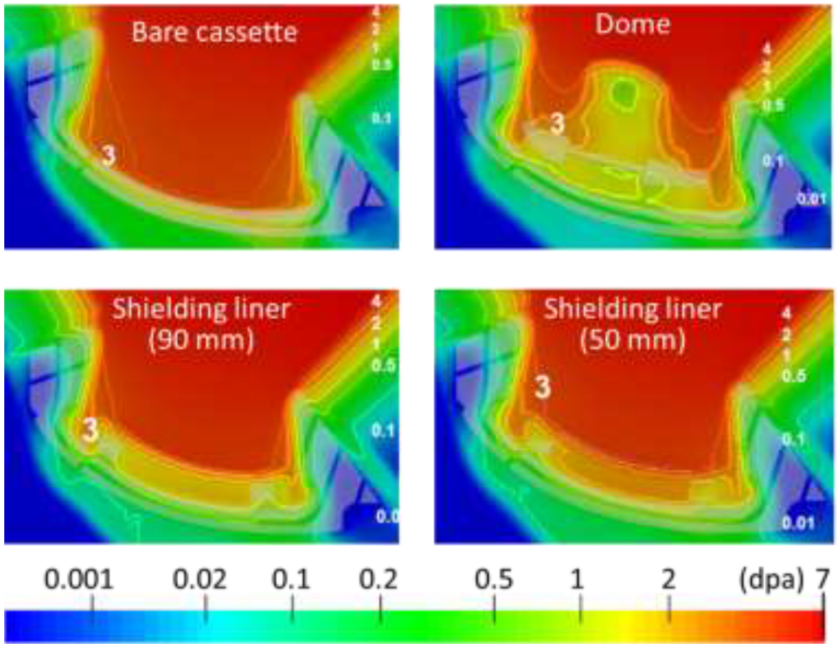

Fig. 14. Spatial distributions of lattice damage generated by neutron irradiation in unit of dpa (displacement per atom) per one full power year (fpy) plotted for four different cases of design options.

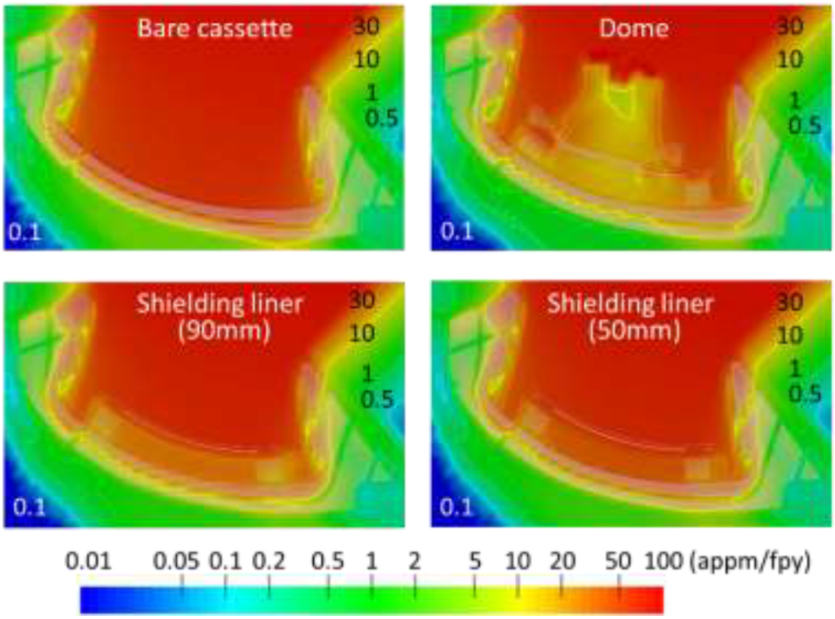

Fig. 15. Spatial distributions of helium production rate by transmutation in unit of appm (atomic parts per million) per fpy together with contour lines of selected concentrations.
Selected positions for the nuclear loading data in Tables 8 and 9. Positions 1 and 2 are at the lower port boundary of the vacuum vessel while 3 and 4 at the upper shell below the pumping duct of the cassette body. (a), (b): Poloidal cut sections at two different toroidal angular positions. (c), (d): Cross section view of the vessel at position 2 and 4, respectively.

1. small dome, large duct (Dome S/Duct L)
2. small dome, medium duct (Dome S/Duct M)
3. small dome, small duct (Dome S/Duct S)
4. medium dome, medium duct (Dome M/Duct M)
5. large dome, medium duct (Dome L/Duct M)
6. small dome, medium duct, baffle (Dome S/Duct M with B)

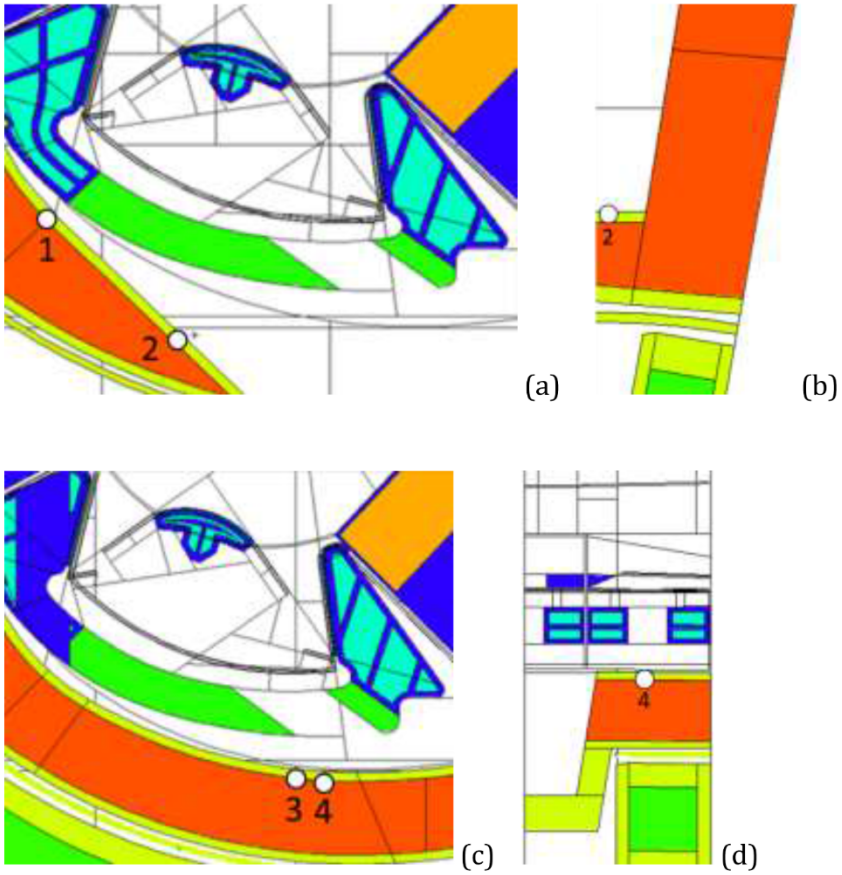

Fig. 15. (*continued*)

Table 7
Maximum production rate of transmuted helium in the Eurofer steel cassette body at six selected locations indicated in Fig. 12. The numbers in parenthesis indicate the ratios to the bare cassette case.

(appm/fpy)	Bare cassette	Dome	SLC (90mm)	SLC (50mm)
Inboard/shadow	31	29 (0.92)	31 (1.0)	32 (1.03)
Inboard/edge	27	27 (0.99)	29 (1.05)	29 (1.07)
Middle/shadow	66	19 (0.28)	32 (0.48)	43 (0.64)
Middle/edge	63	17 (0.26)	35 (0.56)	43 (0.69)
Outboard/shadow	41	29 (0.71)	30 (0.72)	33 (0.80)
Outboard/edge	44	31 (0.70)	31 (0.71)	34 (0.77)

Table 8
Nuclear heating power density in the vacuum vessel (austenitic steel) at three selected locations indicated in Fig. 15. The numbers in parenthesis indicate the ratios to the bare cassette case.

(W/cm^3)	Bare cassette	Dome	SLC (90mm)	SLC (50mm)
Position 1	0.2	0.2 (0.82)	0.2 (0.82)	0.2 (0.91)
Position 2	0.8	0.3 (0.33)	0.4 (0.47)	0.5 (0.57)
Position 3	1.2	0.8 (0.67)	0.6 (0.46)	0.7 (0.60)
Position 4	1.4	1.0 (0.68)	0.8 (0.56)	1.0 (0.70)

Table 9
Cumulative irradiation damage per fpy in the vacuum vessel (austenitic steel) at three selected locations indicated in Fig. 15. The numbers in parenthesis indicate the cumulative irradiation damage dose after 6 fpy.

dpa/fpy	Bare cassette	Dome	SLC (90mm)	SLC (50mm)
(dpa/6 fpy)				
Position 1	0.1 (0.5)	0.06 (0.4)	0.05 (0.3)	0.06 (0.3)
Position 2	0.2 (1.4)	0.06 (0.4)	0.1 (0.6)	0.1 (0.8)
Position 3	0.5 (3.3)	0.4 (2.3)	0.2 (1.2)	0.3 (1.6)
Position 4	0.8 (4.8)	0.6 (3.4)	0.3 (1.8)	0.4 (2.5)

Table 10
Helium production rate per fpy in the vacuum vessel (austenitic steel) at three selected locations indicated in Fig. 15. The numbers in parenthesis indicate the amount of cumulative helium production after 6 fpy.

appm/fpy	Bare cassette	Dome	SLC (90mm)	SLC (50mm)
(appm/6 fpy)				
Position 1	0.8 (5.0)	0. 7 (4.0)	0.6 (3.6)	0.7 (4.0)
Position 2	3.0 (17.8)	0.8 (4.7)	1.2 (7.0)	1.6 (9.7)
Position 3	6.7 (40.4)	5.0 (29.8)	2.4 (14.5)	3.4 (20.6)
Position 4	10.0 (60.0)	7.8 (46.7)	4.2 (25.3)	6.0 (35.7)

Table 11
Nuclear loading of the dome at selected positions as indicated in Fig. 16 (a)

Positions	Nuclear power density (W/cm^3)	Damage dose rate	He production rate
		(dpa/fpy)	(appm/fpy)
1		5.5	
2	8.9	4.4	81.4
3	5.2	1.4	18.9
4	2.6	0.7	8.9

7. large dome, small duct, baffle (Dome L/Duct S with B)
8. extra-large dome, medium duct (Dome 2L/Duct M)

The lengths of the dome extension wings are given in Fig. 4 and the extent of pumping duct is illustrated in Fig. 7.

In Table 14, the nuclear loads estimated at the inboard edge area on the upper surface of the cassette body are given for the eight design variants. The ratio of damage dose rate between the two extreme cases (Dome S/Duct L vs. Dome L/Duct S with B) is about 2.2. It should be noted that the size of the duct opening directly affect the efficiency of gas pumping. Thus, the duct size cannot be simply reduced without compromising pumping efficiency. However, this will not be a critical issue for the cassette body because the maximum damage dose remains below the design limit (6 dpa at 2 fpy) even for the most conservative case (Dome S/Duct L).

Fig. 18 show the spatial distribution of damage dose for three variants where the duct opening was fixed to the medium size (left: Dome S/Duct M, middle: Dome S/Duct M with B, right: Dome 2L/Duct M). The shielding effect caused by either the baffle plates or extension wings is clearly seen as reduced area of red region.

In Table 15, the damage dose rate (per fpy) and cumulative damage at the end of service life of the vacuum vessel (6 fpy) are given. The damage dose values were calculated at the inner shell of the vacuum vessel for the eight design variants. The results clearly show that the vessel can be reasonably protected only in the presence of the baffle plates (and extension wings). This means that employing domes as shielding component necessarily requires assistance of baffle plates not only for protect the pipe connectors but also for shielding the vessel by covering gaps that allow neutron streaming. Both the pumping duct size and the extension of dome wings give the major impact on the damage at the vessel inner shell.

4.5. Nuclear loads in the magnets

The nuclear loads in the underlying magnet coils are given in Table 16, where neutron flux density and nuclear power density are estimated for the two most contrasting design variants, namely, small dome and large duct versus large dome (wing) and small duct with baffle plates. The result shows that even the best shielding case does not satisfy the design criterion which requires that volumetric nuclear heating in the superconducting magnets be lower than 0.05 mW/cm^3. This negative feature indicates that an overall design revision is needed for the whole cassette system to enhance the shielding performance for fulfilling the design criteria for the vessel and the magnets.

4.6. Nuclear loads in the divertor targets

Although the nuclear loads in the divertor targets are not the primary indicator of shielding performance of divertor, the information on these data gives designers fundamental guidelines with regard to permissible operation condition and achievable lifetime of the critical plasma-facing component. Particularly, the irradiation damage dose has major impact on material performance and structural integrity of the most thermally loaded component, targets.

In Table 17, the cumulative damage dose after 2 fpy estimated for six selected positions (see Fig. 19) on the inboard and outboard target plates are given. The three materials listed in the table denote the tungsten armour block, the copper alloy cooling pipe and the steel fixation legs, respectively. As expected, the upper edge regions of both targets near the X-point experience the highest damage compared to the lower parts including the strike point. For example, in the tungsten armour and the copper cooling pipes, the ratio of damage between the upper edge and strike point amounts to 2.9 (inboard) or 4.7 (outboard). The most critical concern is the damage in the cooling pipe being the only pressurized structural material. The maximum damage in the pipe reaches almost 15-17 dpa at the end of the envisaged lifetime (2 fpy), which is considerably high compared to the expected damage in ITER divertor. For designing the targets, it should be assured that the damage level be acceptable for the pipes at the specified cooling condition where coolant temperature is supposed to range from 130°C to 140°C. Unfortunately, no irradiation test data is available for the copper alloy at such high dpa level [33]. Thus, it seems very difficult to make any judgement as to whether the predicted damage level is acceptable for the operation conditions and the lifetime under consideration. Note that

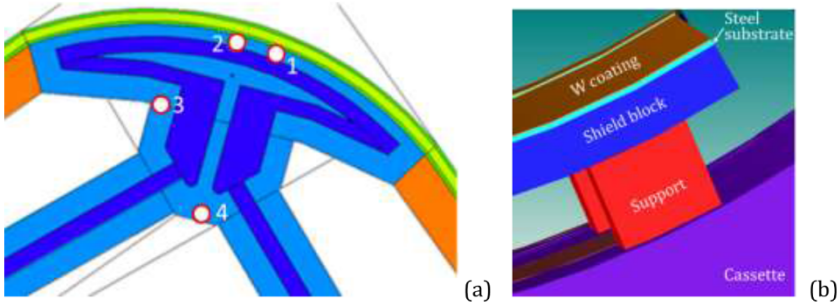

Fig. 16. Selected positions for the nuclear loading data in Table 11. In (a) position 1 indicates the area of maximum nuclear loading in the dome.

Table 12
Nuclear loading of the SLC (shield block: 90mm) in the selected parts as indicated in Fig. 16 (b).

Positions	Nuclear power density (W/cm^3)	Damage dose rate (dpa/fpy)	He production rate (appm/fpy)
W coating	20.1	1.5	0
Steel substrate	6.3	4.1	59.2
Shield block	5.4	2.5	45.7
Support	3.3	1.2	26.7

Table 13
Nuclear loading of the SLC (shield block: 50mm) in the selected parts as indicated in Fig. 16 (b).

Positions	Nuclear power density (W/cm^3)	Damage dose rate (dpa/fpy)	He production rate (appm/fpy)
W coating	19.8	1.5	0
Steel substrate	6.2	4.1	57.9
Shield block	3.3	2.9	49.6
Support	4.0	1.6	33.7

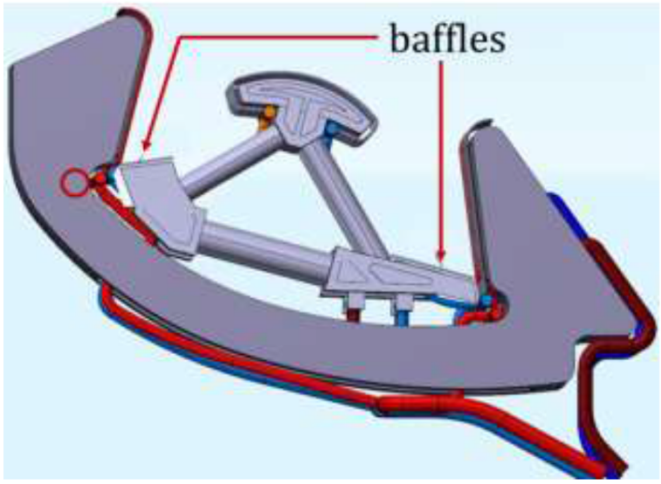

Fig. 17. Two baffles introduced optionally as subcomponent.

the irradiation effects (e.g. hardening) of CuCrZr alloy tend to be readily saturated already in the early stage of irradiation (0.1-1 dpa) [32]. Whether such an early saturation behaviour will continue to hold beyond 10 dpa is still an open question. This lack of critical materials data urgently necessitates a dedicated irradiation testing campaign for the divertor materials in near future.

The damage level in the steel legs in the upper edge region exceeds the permissible limit (6 dpa). For reducing the damage, the outline configuration of the breeding blanket and cassette will need to be modified to allow shadowing by the blanket edges.

5. Summary and Conclusions

1. In this article, a first dedicated neutronics study for the divertor (interim version) of the European DEMO power plant is reported where the nuclear shielding performance of two different types of shielding components (i.e. dome vs. shielding liner) were evaluated and compared. The case of bare cassette (i.e. without shielding component) was also investigated as reference.
2. As objectives of this comparative neutronics study, nuclear heating, irradiation damage and helium production in the cassette body, the vacuum vessel and the own body of the shielding components were assessed.
3. The bare cassette cannot provide required shielding for the vacuum vessel and thus is not applicable. The cause of exceedingly high radiation loads is unhindered neutron streaming through the large pumping duct opening locating at the middle part of the cassette body.
4. Both the dome and the shielding liner are able to significantly reduce the nuclear loads in the cassette body and the vacuum vessel.
5. For the cassette body (Eurofer steel), the maximum irradiation damage dose expected at the end of the envisaged component lifetime (2 fpy) is still below the critical design limit (6 dpa).
6. For the vacuum vessel (316LN steel), the maximum irradiation damage dose expected at the end of the component lifetime (6 fpy) is mostly below the critical design limit (2.75 dpa) but there is a small local hot spot on the upper surface underneath the downward pumping duct opening where the dose (3.4 dpa) exceeds the limit under the dome. Under the shielding liner, however, the hot spot remains uncritical (1.8-2.5 dpa).
7. The intensity of the nuclear loads strongly depend on the geometry and the dimension of the shielding components as well as the pumping duct. For example, the shielding performance of the dome can be reasonably improved by attaching extension wings at the dome edge or using baffle plates to cover the duct opening which allow reduction of nuclear loads below the critical design limit even with a large pumping duct.
8. The most critical feature is the nuclear loads (particularly damage) occurring in the own body of the shielding components. The maximum damage dose in the steel (Eurofer) heat sink of the dome (10 dpa) and of the shielding liner (8 dpa) far exceeds the design limit (6 dpa) at the end of the lifetime (2 fpy). This loading feature seems to be a critical design issue as the shielding components are supposed to act as a kind of nuclear firewall at the forefront of the radiation loads and as such will not be able to be protected by additional components.
9. Another critical feature, which may be an issue of concern, is the relatively high production rate of helium as transmutant. The expected helium concentration at the end of the lifetime is by a few orders of magnitude larger than the assumed critical limit for re-welding.

Table 14
Nuclear loading at the inboard edge area on the upper surface of the cassette body estimated for 8 different combinations of dome wing extension and pumping duct size.

Variant	Neutron flux density (10^{14} n/cm^2·s)	Nuclear power density (W/cm^3)	Damage dose rate (dpa/fpy)
Dome S/Duct L	1.5	3.5	2.6
Dome S/Duct M	1.6	3.4	2.5
Dome S/Duct S	1.5	3.4	2.1
Dome M/Duct M	1.4	3.4	2.5
Dome L/Duct M	1.3	3.0	2.1
Dome S/Duct M with B	1.0	2.2	1.8
Dome L/Duct S with B	0.9	1.9	1.2
Dome 2L/Duct M	1.2	2.8	2.0

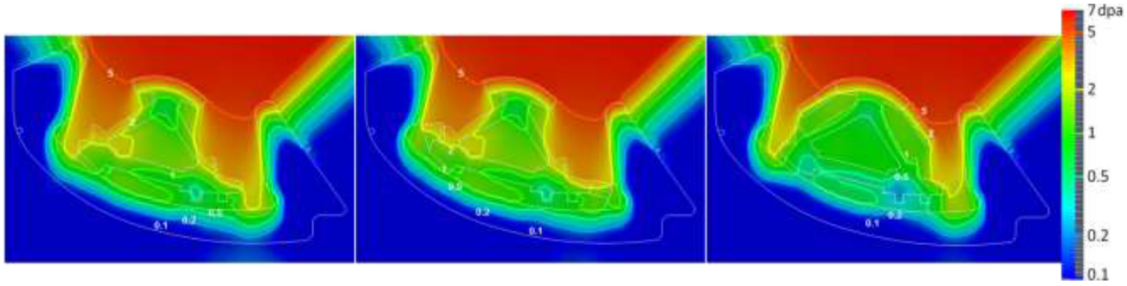

Fig. 18. Spatial distribution of damage dose for three variants where the duct opening was fixed to the medium size (left: Dome S/Duct M, middle: Dome S/Duct M with B, right: Dome 2L/Duct M).

Table 15
Maximum cumulated damage in the inner shell of the vacuum vessel estimated for 8 different combinations of dome wing extension and pumping duct size.

Variant	dpa/fpy	dpa/6 fpy
Dome S/Duct L	0.86	5.16
Dome S/Duct M	0.59	3.51
Dome S/Duct S	0.59	3.54
Dome M/Duct M	0.56	3.36
Dome L/Duct M	0.50	3.00
Dome S/Duct M with B	0.45	2.70
Dome L/Duct S with B	0.36	2.16
Dome 2L/Duct M	0.48	2.88

Table 16
Nuclear loads in the superconducting magnet coils near a divertor cassette estimated for the two most contrasting design variants.

Variant	Neutron flux density (10^{12} n/cm^2·s)	Nuclear power density (mW/cm^3)
Dome S/Duct L	1.5	9
Dome L/Duct S with B	0.8	4
Allowable max. limit		0.05

Table 17
Cumulative damage dose after 2 fpy estimated for six selected positions (see Fig. 19) on the inboard and the outboard target plates (W: armour block, CuCrZr: cooling pipe, Eurofer: fixation legs).

Position	W (dpa/2 fpy)	CuCrZr	Eurofer
1	0.8	3.6	2.4
2	1.6	7.4	4.8
3	3.8	16.8	8.6
4	1.0	5.1	3.3
5	1.2	5.5	3.4
6	2.8	14.9	7.4

10. The nuclear heating power density in the lower part of the superconducting magnet coil near the lower port is shown to be too high to be acceptable by three orders of magnitude. This requires improved shielding also for the lower port.
11. The damage dose in the plasma-facing components of the inboard and outboard targets is considerably higher than that of the ITER divertor targets. The maximusm damage dose in the structural material (copper cooling pipe) is not covered by the currently available structural design codes.

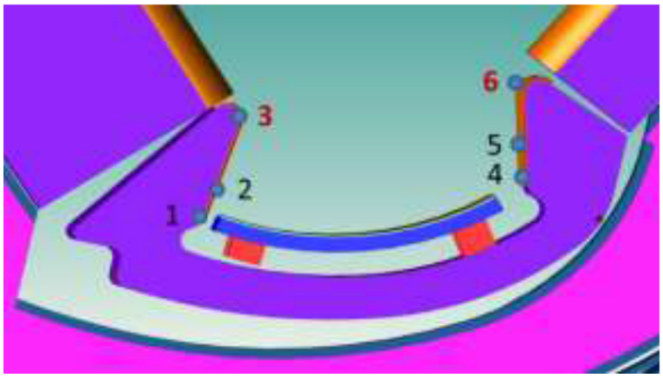

Fig. 19. Six selected positions on the outboard (left) and inboard (right) target plates for which cumulative damage dose were estimated.

Declaration of Competing interests

The authors declare that they have no known competing financial interests or personal relationships that could have appeared to influence the work reported in this paper.

Acknowledgment

This work has been carried out within the framework of the EUROfusion Consortium and has received funding from the Euratom research and training program 2014-2018 and 2019-2020 under grant agreement No 633053. The views and opinions expressed herein do not necessarily reflect those of the European Commission.

References

[1] J. Wesson, Tokamaks, 4 ed, Oxford University Press, 2011, pp. 490–504.
[2] R.A. Pitts, J. Nucl. Mater 415 (2011) S957–S964.
[3] C. Bachmann, et al., Fus. Eng, Des 112 (2016) 527–534.
[4] F. Cismondi, et al., Fus. Eng, Des 124 (2017) 562–566.
[5] J.H. You, et al., Fus. Eng, Des 109-111 (2016) 1598–1603.
[6] J.H. You, et al., Nucl. Mater. Ener 9 (2016) 171–176.
[7] J.H. You, et al., Fus. Eng, Des 124 (2017) 364–370.
[8] E. Gaganidze, et al., Fus. Eng, Des 88 (2013) 118–128.
[9] V. Barabash, et al., J. Nucl. Mater 283-287 (2000) 138–146.
[10] Ch. Linsmeier, et al., Nucl. Fus 57 (2017) 09200760pp.
[11] M. Li, et al., Fus. Eng, Des 89 (2014) 2716–2725.
[12] J.H. You, J. Nucl. Mater 375 (2008) 283–289.
[13] M. Fursdon, et al., Fus. Eng, Des 147 (2019) 111234.
[14] P. Frosi, et al., Fus. Eng, Des 124 (2017) 628–632.
[15] P. Frosi, et al., Fus. Eng, Des 138 (2019) 119–124.
[16] P.A. Di Maio, et al., Fus. Eng, Des 136 (2018) 1588–1592.
[17] P. A. Di Maio, et al., Fus. Eng. Des., https://doi.org/10.1016/j.fusengdes.2018.12.024.
[18] RCC-MRx AFCEN Edition2015.
[19] C. Bachmann, private communication.
[20] G. Federici, et al., Fus. Eng, Des 136 (2018) 729–741.
[21] D. Marzullo, et al., Fus. Eng, Des 124 (2017) 649–654.
[22] D. Marzullo, et al., Fus. Eng. Des. https://doi.org/10.1016/j.fusengdes.2019.01.120.
[23] M. Merola, et al., Fus. Eng, Des 96–97 (2015) 34–41.
[24] J.H. You, et al., Nucl. Mater. Ener 16 (2018) 1–11.
[25] SpaceClaim Tutorials, http://www.spaceclaim.com/de/Support/Tutorials/Essentials.aspx.
[26] Y. Wu, et al., Fus. Eng, Des 84 (2009) 1987–199.
[27] G. Mazzone, et al., Fus. Eng, Des 124 (2017) 655–658.
[28] https://www-nds.iaea.org/public/download-endf/DXS/SS-316_dpa-XS/ACE/.
[29] X-5 Monte Carlo Team, MCNP - A General Monte Carlo N-Particle Transport Code (V5), Los Alamos National Laboratory, Los Alamos, USA, 2003.
[30] JEFF-3.2 evaluated data library - Neutron data, Nuclear Energy Agency, http://www.oecd-nea.org/dbforms/data/eva/evatapes/jeff_32/.
[31] T. Wilcox, "MCNP6 Advanced Tallies Tutorial", ANS RPSD-2014, LA-UR-14-27128 (2014).
[32] V. Barabash, et al., J. Nucl. Mater 367–370 (2007) 21–32.
[33] ITER SDC-IC Appendix A G 74 MA 8 01-05-28 W 0.22012.